Structure and dynamics of ER: minimal networks and biophysical constraints

Congping Lin[*], Yiwei Zhang[†], Imogen Sparkes[‡], Peter Ashwin[*]

(June 10, 2014)

Abstract

The Endoplasmic Reticulum (ER) in live cells is a highly mobile network whose structure dynamically changes on a number of timescales. It is unclear in any system the role of such drastic changes although there are correlations with ER function. A better understanding of the fundamental biophysical constraints on the system will allow biologists to determine the effects of molecular factors on ER dynamics. Previous studies have identified potential static elements which the ER may remodel around. Here, we use these structural elements to assess biophysical principles behind the network dynamics. By analyzing imaging data of Tobacco leaf epidermal cells under two different conditions: native state (control) and latrunculin B (treated), we show that the geometric structure and dynamics of ER networks can be understood in terms of minimal networks. Our results show that the ER network is well-modelled as a locally minimal-length network between the static elements that potentially anchor the ER to the cell cortex over longer timescales; this network is perturbed by a mixture of random and deterministic forces. The network need not have globally minimum length; we observe cases where the local topology may change dynamically between different "Euclidean Steiner Network" topologies. The networks in the treated cells are easier to quantify as they are less dynamic (the treatment suppresses actin dynamics) but the same general features are found in control cells. Using a Langevin approach we model the dynamics of the non-persistent nodes and use this to show that the images can be used to estimate both local viscoelastic behavior of the cytoplasm and filament tension in the ER network. This means we can explain several aspects of the ER geometry in terms of biophysical principles.

Keywords: Endoplasmic Reticulum; Geometry; Dynamics.

1 INTRODUCTION

The endoplasmic reticulum (ER) is the largest membrane-bound organelle in most eukaryotic cells, and spreads throughout the cytoplasm as one highly complicated interconnected

[*]Mathematics Research Institute, Harrison Building, University of Exeter, Exeter EX4 4QF, UK
[†]Facultad de Matemáticas, Pontificia Universidad Católica de Chile, Santiago 7820436, Chile
[‡]Biosciences, Geoffrey Pope Building, University of Exeter, Exeter EX4 4QD, UK

network that surrounds a single lumen [1]. It serves important roles in protein and phospholipid synthesis, quality control and export, and calcium storage [2]. Dysfunction of the ER is linked to a range of neurological disorders including Alzheimer's disease [3, 4]. The functional role of the ER is related to its morphological structure which is composed of an intricate connected network of tubules and cisternae [5]. The ER tubules have high mean curvature in cross section, whereas cisternae are dilated tubules comprised of extended regions of parallel, flat membrane bilayers that are stacked over each other with high curvature constrained to the periphery of the cisternae [5, 6]. Tubules grow and shrink, and undergo lateral sliding to form closed polygons as well as readily changing into cisternae. Research suggests that a dynamic ER network allows the ER to establish and maintain functional contacts with membrane-bound organelles as they move, and to adapt to changes in cell morphology during cell migration, differentiation, and polarization [7, 8]. The movement of the ER network is regulated by the cytoskeleton and molecular motors [5, 6, 9, 10, 11]. In plant cells, depolymerisation of the actin cytoskeleton inhibits ER remodelling. ER dynamics can also be influenced by physical properties of ER surface tension [12] and the rheological behavior of cytoplasm which is usually intermediate between the two limit behaviors of a viscous liquid and an elastic solid [13, 14].

Due to the highly dynamic and intricate nature of the ER network, quantifying changes has proven difficult. Quantitative analysis so far has mainly focused on tubule length [15, 16, 17, 18], diameter [18] and branching properties [16, 17]. These types of studies tend to be carried out on either fixed tissue or after treatment with cytoskeletal inhibitors and so are based on networks which are no longer actively remodelling. In order to start unpicking and quantifying elements in an actively remodelling network, Sparkes *et al* [9] developed an image analysis method for pulling out the persistent or static elements of the ER network in tobacco leaf epidermal cells. Persistent tubules and cisternae were observed as well as static nodes or points, all of which may have important roles in anchoring the network to the plasma membrane [9, 19, 20]. In addition, Bouchekhima *et al* have analyzed ER dynamics by measuring displacement of nodes and average velocity [21, 22]. Many questions remain concerning the biophysical mechanisms underlying dynamical changes and the biological significance of these changes [5, 23]. One of the many unresolved questions relates to the functional role of the ER forming such an intricate thermodynamically unfavourable network structure in the cell. Without better tools to quantify network dynamics these basic types of questions will remain unresolved.

In nature, minimal length or surface structures are prevalent - they provide economical ways of joining or supporting structures (e.g. the skeletons of radiolarians or cell transport networks), and biophysical mechanisms such as surface energies or interfacial tensions easily drive processes that result in minimal surfaces [24]. The problem of finding a minimal surface with a given boundary, known as the Plateau's problem [24]. Indeed, the structure of tightly stacked ER sheets (cisternae) has been modelled as a minimum of elastic energy of sheet edges and surface [25]. In this paper, we focus on the ER tubules which form networks between persistent points. Finding a minimal network between points is known as the Euclidean Steiner tree problem - a low dimensional case of Plateau's problem [24]. For the ER tubule networks, we show they can be well described as a perturbed *Euclidean Steiner network* (ESN) by analyzing the structure of *in vivo* ER networks. We use a Langevin approach to model the dynamics of non-persistent nodes in a small network and are able to

use this modelling methodology to estimate biophysical quantities of the ER in the living cell, including both the local viscoelastic behavior of the cytoplasm and the filament tension of the ER network.

2 MATERIALS AND METHODS

The live cell imaging data of ER network dynamics analyzed in this paper is from tobacco leaf epidermal cells (taken from [9]) in two cases: a native state with active remodelling (referred to as control) and a latrunculin B treated sample where the ER network is relatively static in comparison (referred to as treated). Both experimental ER networks are transiently expressing green fluorescent protein (GFP) retained in the ER lumen. The GFP marker fills the entire ER network throughout the cortex of the cell and is shown as grey levels in figures. The ER recordings for both treated and control are composed of $N = 50$ frames with a time-resolution $1.6s$ between frames and a spatial resolution of $0.11\mu m$ per pixel. Examples of networks are illustrated in Fig 1 where markers and lines are for the presentation of geometric graphs simplifying the ER networks for quantitative analysis.

2.1 Euclidean Steiner Networks

In this section, we introduce the notion of *Euclidean Steiner network (ESN)* that is a slight generalization of a Steiner tree. First we recall the definition of Steiner tree. A tree between a number of fixed points is a cycle-free connected graph having these points as its nodes and a minimal spanning tree is a tree whose total length (sum of the lengths of all its lines) as small as possible. However, one can often construct a shorter spanning tree between these fixed nodes $u_1, u_2, \cdots, u_P$ by including extra nodes $x_1, x_2, \cdots, x_M$ [26]. By minimizing over the trees on extra points, local minima are called *Steiner trees* (ST) where the fixed nodes are called *terminals* and the additional points are called *Steiner points* while the globally minimal is called the *Steiner minimal tree* (SMT). More precisely, a (Euclidean) *Steiner tree* (ST) as a tree whose length cannot be shortened by a small perturbation of Steiner points, even when splitting is allowed. By splitting a node v, one disconnects two or more of the lines at v and connects them instead to a Steiner point. There could be several STs between a set of terminals, and these differ in topology (i.e., a connection description specifying which pairs of points have a connecting line); A and B in Fig 2 are two STs with the same four terminals.

Consider a network G connecting a set of terminals and possibly additional points on the plane. We say G is an *Euclidean Steiner network* (ESN) between these terminals (and the additional points are Steiner points) if no small perturbation of Steiner points will decrease the length, even if splitting is allowed. In contrast to a ST, an ESN can have cycles (see C,D in Fig 2). Clearly, the shortest length ESN must be the SMT between terminals and a cycle-free ESN is a ST. Analogous to STs [27], for ESNs all Steiner points are of degree three (i.e., lines radiating outwards) and have angles 120° between edges, while the terminals must be of degree at most three and must have angles not less than 120° between edges that meet there. Steiner points in STs and ESNs in this paper are determined by GeoSteiner [28].

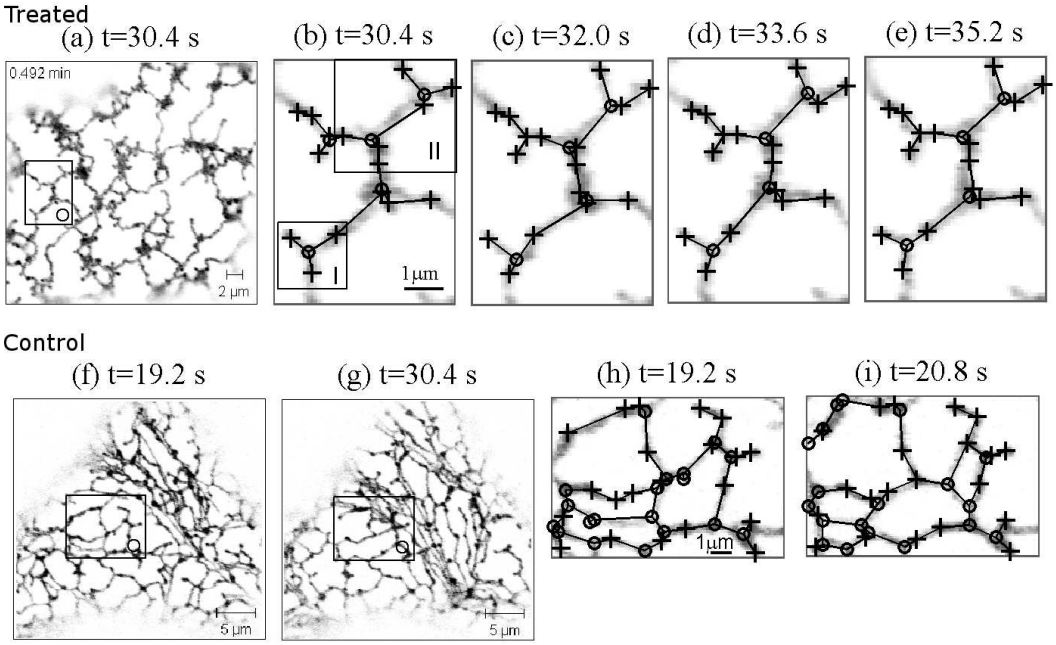

Figure 1: Illustration of the treated (top panels) and control (bottom panels) ER network and local dynamics. The rectangle Region O in (a) and (f) highlights a region with no cisternae. In control, (f) and (g) show a transition between ER tubule and cisternae in Region O. Details of the dynamics in Region O are shown in (b)-(e) for treated and (h)-(i) for control, with the geometric graphs (where markers '+' are persistent and 'o' are non-persistent nodes while lines are edges) abstracted from an image processing method as described in Section 2.2. Sub-regions I and II in (b) are used for modeling the dynamics of treated ER networks. The imaging data is taken from [9] (`www.plantcell.org`, Copyright American Society of Plant Biologists); dynamics in Region II is shown in Movie 1 and in control is shown in Movie 2.

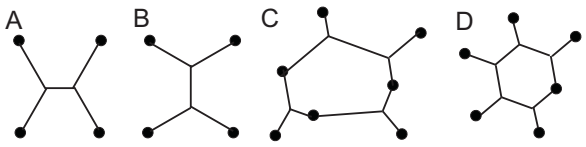

Figure 2: Examples of Steiner trees A,B and Euclidean Steiner networks (ESNs) with cycles C,D; terminals are shown in bold dots and Steiner points are junctions between connecting lines. A,B are the two Steiner trees for the same terminals. In all cases, the angles at Steiner points are 120° and the angles at terminals are at least 120°.

2.2 Image processing methods

We briefly outline the image processing method we use to dynamically extract the terminals and graphs from the sequence of 2D imaging data of [9]. The method is similar to that in [22]; however, we distinguish between persistent and non-persistent nodes; persistent nodes (that are static over a give time duration) relate to the static nodes isolated by persistency mapping and are thought to be of biological significance in the ER structural organization [9].

Thus, at a given time the graph is composed of a number of persistent nodes $\{p_1, p_2, \cdots, p_P\}$ that are present in the given time duration and a number of non-persistent nodes $\{s_i\}_{i=1}^{k(t)+m(t)}$ which is the union of the branching junctions $\{b_i(t)\}_{i=1}^{k(t)}$ and the degree one nodes $\{o_i(t)\}_{i=1}^{m(t)}$. Branching and/or degree one nodes and their number may change during the remodelling of the ER.

The persistent nodes are found by (a) taking average pixel intensities over a fixed time duration (we use a time duration $80s$ of the entire movie as default unless otherwise stated), (b) smoothing this averaged image by a Gaussian filter $K_{r,\sigma}$ of kernel size r and standard variation σ and (c) finding the local maximum (using an 8-connected neighborhood) in the smoothed images after applying a threshold I_1. We use the parameters $r = 3$, $\sigma = 0.8$ and threshold $I_1 = 110$; the choice of these parameters is discussed in Supplementary Material (Section A).

To obtain the non-persistent nodes, we smooth each image using the Gaussian filter $K_{r,\sigma}$ followed by thresholding with a threshold I_2 to give a binary image. We then find the skeleton (of one-pixel width and the same topology as the binary image) using a thinning algorithm [29] which gives "non-persistent" degree one (ends in the skeleton) and branching (junctions in the skeleton) nodes that are not in the set of persistent nodes; we assume that the persistent nodes are always in the network by rounding the persistent nodes to the closest point on the skeleton. We use $I_2 = 20$ for the treated ER and $I_2 = 35$ for the control; the choice of these parameters is discussed in Supplementary Material (Section A).

Since we are testing whether ER tubules are connected and conform to an ESN, we are focusing on a relatively simple region of the ER network which is devoid of cisternae with the long term plan of extending the study to cover both morphological forms of the ER (tubules and cisternae). For the treated ER, we have studied the network within the Region O of Fig 1(a). In this region, the non-persistent nodes move and connect to other nodes within the region; see Fig 1(b-d). For the control ER, due to its complex spatial dynamics as well as its rapid transition between tubular and cisternal forms (e.g. seen from Fig 1(f,g)), we choose different regions with no cisternae at different static images in the recording, such as Region O in Fig 1(f), to study its network properties. In a chosen region, we take the largest connected component in the skeleton and the nodes on the skeleton. Each pair of nodes on the skeleton is connected by an edge if there is a path in the skeleton connecting the two nodes without passing other nodes. The length of each edge is given by the Euclidean distance between two nodes (i.e., the length of the line).

This process delivers a time-dependent sequence of geometric graphs $G(t) = (V(t), E(t))$ between a set of persistent nodes $V_p = \{p_i\} \subset V(t)$ that are static throughout the movie, a set of additional non-persistent nodes $V_s = \{s_i(t)\} \subset V(t)$ that vary in position and number, and a set of edges $E(t) = \{e_i(t)\}$ that connect the nodes. Our image processing method gives about 99.7% (95.3%) of pixels among the lines in the abstracted graphs for treated (control) ER networks agree with that in the binary images before skeletonization. This indicates that the ER filaments between nodes are well described by straight lines.

3 RESULTS

We examine some properties of the instantaneous networks in Section 3.1 and test the hypothesis that they are close to ESNs, before looking at the dynamics of the networks for the treated ER in Section 3.2 and the control ER in Section 3.3 and biophysical properties of the ER in Section 3.4.

3.1 Instantaneous ER networks

Fig 3(top) compares the number of nodes in the treated and control ER networks for the chosen regions, considering the population of graphs $G(t)$ over all instants of time. The average number of total nodes in a given unit area are similar between treated and control ER. Moreover, in both networks, persistent nodes are mainly non-branching (i.e., connecting 1 or 2 tubules) while non-persistent nodes are mainly branching. However, the treated ER has more persistent nodes than non-persistent nodes in a unit area whereas the control ER has an approximately equal number of both. Comparing treated and control, the control ER has more non-persistent nodes per unit area than the treated ER. These observations are in agreement with the dramatic dynamic changes seen in the control network versus the treated sample. In addition, the mean edge length in the treated ($1.34 \pm 0.033 \mu m$ (N=986)) and control ($0.96 \pm 0.013 \mu m$ (N=2312)) ER networks is similar.

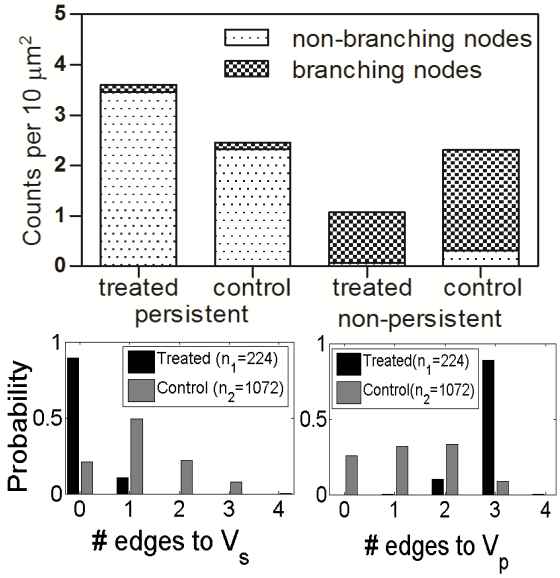

Figure 3: Node and edge analysis of abstracted treated and control ER networks in chosen regions over the analyzed movies. Top: number of persistent (left two bars) and non-persistent (right two bars) nodes per unit area ($10 \mu m^2$). The majority of persistent (non-persistent) nodes are non-branching (branching). In the treated ER, 77% are persistent nodes while in the control the number of persistent and non-persistent nodes are approximately equal. Bottom: Distribution of the number of edges from a non-persistent node to non-persistent nodes V_s (left) and to persistent nodes V_p (right).

Note that non-branching nodes (mainly persistent nodes) have one or two edges while branching nodes (mainly non-persistent) mainly have three edges both for treated and control ER (a branching node will have less than three edges if is links with tubules extended outside the chosen region). To further clarify the linking structure between nodes, Fig 3(bottom) shows that for the treated ER networks, a majority ($\sim$ 90%) of non-persistent nodes are connected to 3 persistent nodes and no others while for the control ER, the number of edges between different types of nodes is much more homogeneous. By contrast, Fig S3 shows that the treated and control ER do not show significant difference in the distribution of the number of edges from a persistent node.

Fig 4(top) shows that the angles at non-persistent nodes for both treated and control follow a normal distribution with a mean around 120° and a standard variation around 25°. Furthermore, a two-sample Kolmogorov-Smirnov test suggests that the two are from the same normal distribution. Fig 4(bottom) shows that angles of persistent nodes are predominantly larger than 120° for both treated and control ER. This agrees well with the hypothesis that the networks are perturbed ESNs, and that the non-persistent branching nodes are perturbed Steiner points.

Moreover, Fig 5 (and Fig S4(a-b)) show examples of abstracted self-contained ER networks that are clearly close to an ESN whose terminals are the persistent and degree one nodes. In particular, for the treated ER networks where terminals are consistent in the entire movie, we further show in Fig S4(c-d) the distribution of branching nodes and the peaks of the distribution are close to Steiner points in the corresponding Steiner minimal tree. This also suggests that the instantaneous ER networks are well modelled as perturbed ESNs.

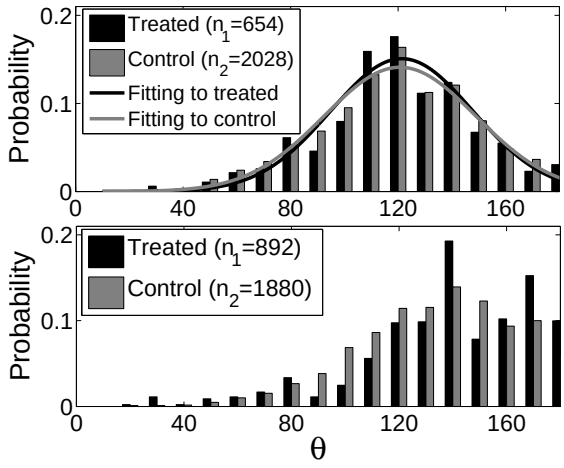

Figure 4: Angle distribution for non-persistent (top) and persistent (bottom) nodes for both treated (black) and control (grey) ER networks in chosen regions. The smooth curves show best Gaussian fits to the distribution from the corresponding treated (black; with a mean 121.4° and standard variation 25.7) and control (grey; with a mean 120.8° and standard variation 28.3) networks. For persistent nodes, 77.5% (69.2%) of angles are over 120° in treated (control) ER networks.

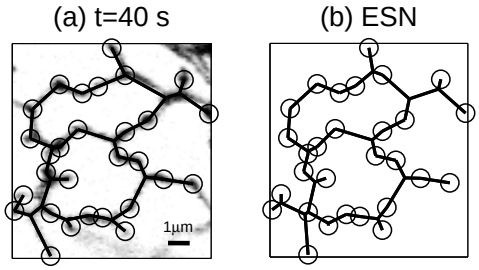

Figure 5: The comparison of a control ER network (a) together with the abstracted geometric graph to the Euclidean Steiner network (b) with terminals (circles) being the persistent and degree-one nodes from (a). Non-persistent nodes in (a) are not connected with nodes outside the region. The imaging data is taken from [9].

3.2 The treated ER network dynamics

We focus on the network dynamics observed in Region O in Fig 1, where the region is chosen to be away from any cisternae of the ER. As the persistent nodes are static, and we can describe the network dynamics via movement of the non-persistent nodes and changes of the network topology.

Section 3.1 suggests that non-persistent branching nodes can be thought of as Steiner points that reduce the total length of the graph. We thus propose a simple model for the dynamics of the graph using a Langevin equation to characterize the motion of non-persistent nodes (ER junctions) $x_i(t) \in \mathbf{R}^2$ (unit μm) for $i = 1..M$ as

$$\frac{dx_i}{dt} = -a\nabla_{x_i} f(x_i, \ldots, x_P) + \sqrt{2\sigma}\xi(t) \tag{1}$$

where $f(x_i, \ldots, x_P)$ represents the total length in the network between persistent and the given non-persistent nodes (the network topology will be implicitly inferred from node locations). In the mode, there are a drift coefficient a (unit $\mu m/s$) and a diffusion coefficient σ (unit $\mu m^2/s$) modulating white noise $\xi(t)$ with zero mean and autocorrelation $\langle \xi(t)\xi(t') \rangle = \delta(t - t')$. A physical interpretation of these parameters is discussed in Section 3.4. In the following subsections, we examine the dynamics in regions I and II highlighted in Fig 1(b).

3.2.1 Network dynamics in Region I

This region contains three persistent nodes and one non-persistent node and the topology between the nodes remains the same in the movie, i.e., the non-persistent node x is connected to three persistent nodes $p_i \in \mathbf{R}^2$ for $i = 1..3$. In this case the total network length is

$$f(x) = \sum_i |x - p_i|$$

where $|\cdot|$ denotes the Euclidean norm in $\mathbf{R}^2$ and the gradient $\nabla_x f(x) = \sum_i \frac{x-p_i}{|x-p_i|}$. Using the method in Section 2.2, we obtain a time series $x(n\delta), n = 1, \ldots, N$ for the positions of

the non-persistent node with a time step $\delta = 1.6s$. We estimate the diffusion coefficient $\sigma \approx 0.008 \pm 0.001 \mu m^2/s$ ($N = 50$) via quadratic variation [30] as

$$\sigma \approx \frac{1}{2Nd\,\delta} \sum_{n=1}^{N-1} |x((n+1)\delta) - x(n\delta)|^2 \tag{2}$$

where $d = 2$ is the dimension of the x and an asymptotically normal distribution for $|x((n+1)\delta) - x(n\delta)|^2$ from [31] (see Supplementary Material for details). Meanwhile, we estimate the drift coefficient $a \approx 0.2 \pm 0.04 \mu m/s$ ($N = 50$) by maximizing the approximated log-likelihood [32]

$$L_N(a) = \frac{1}{2\sigma} \left(-a \sum_{n=1}^{N-1} \langle \nabla f(x(n)), (x(n+1) - x(n)) \rangle - a^2 \frac{\delta}{2} \sum_{n=1}^{N-1} \langle \nabla f(x(n)), \nabla f(x(n)) \rangle \right) \tag{3}$$

which gives

$$a = -\frac{\sum_{n=1}^{N-1} \langle \nabla f(x(n)), (x(n+1) - x(n)) \rangle}{\sum_{n=1}^{N-1} \delta |\nabla f(x(n))|^2} \tag{4}$$

and an asymptotically normal distribution for a from [33] (see Supplementary Material for details). Linearizing this Langevin equation (1) gives a stochastic differential equation that models the dynamics of the non-persistent node as perturbed Steiner point, which can be simulated and solved analytically. The above estimations of the parameters in (1) agree well with the estimation on its linear part (see Supplementary Material for details).

The Langevin model with the estimated parameters well captures the ER dynamics in region I, through the comparison to the abstracted ER network dynamics in three different ways; (a) the angle distribution for the non-persistent nodes, (b) the time-dependent total length $f(x(t))$ and (c) the position dynamics of the non-persistent node $x(t)$. Indeed the total length from a simulation of Eq (1) oscillating above the length of the corresponding SMT is similar to that in the abstracted graphs; see top panels in Fig 6. Meanwhile, Fig S5 shows good agreement of numerical simulation for the positions and angles of non-persistent nodes.

3.2.2 Network dynamics in Region II

Region II in Fig 1(b) contains six persistent nodes and more than one ST topology is possible (topology changes are not present in Region I). Possible connection structures between these nodes are shown in Fig 7(top) while Fig 7(bottom) shows four different STs corresponding to four observed ER network topologies. All STs with these 6 terminals have two Steiner points. The time-dependent length shown in Fig 6(bottom) illustrates that this length may oscillate about the (local) STs, but may also change between different ST topologies. Analogous to the dynamics in Region I, the positions of the non-persistent nodes oscillate around the positions of Steiner points for the STs and the angles of non-persistent nodes well fit a normal distribution with mean around 120° (see Fig S6 in supplementary material).

The transition between topologies may associate with creation of additional non-persistent nodes. Indeed, Fig S7 indicates that such additional nodes can appear during transitions -

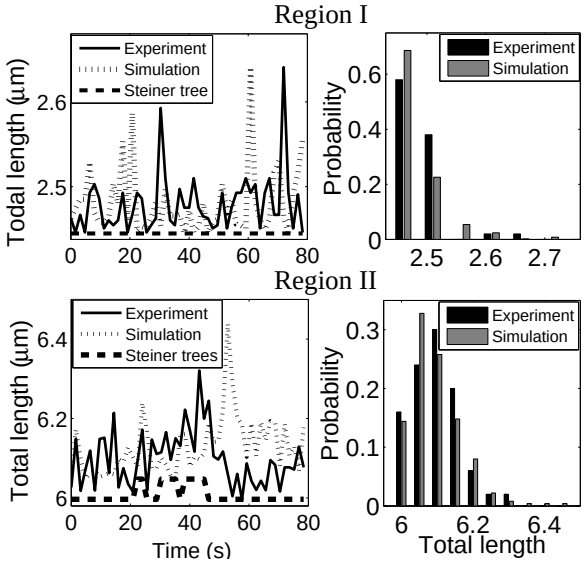

Figure 6: Total length of abstracted graphs from experimental data, numerical simulation of the Langevin equation (1) with an initial condition from the first frame, and the corresponding Steiner minimal tree in Region I (top) and II (bottom) highlighted in Fig 1(b). The corresponding length distribution are given on its right panel and the two sample Kolmogorov-Smirnov tests suggest the total length distribution calculated from experiment and simulation is from the same distribution in each region. Parameters $\sigma = 0.008\mu m^2/s$ and $a = 0.2\mu m/s$ are used in simulations. Observe the periods of time between 20s and 45s where the topology "flips" to be close to a Steiner tree with a different topology in Region II.

this additional node in Region II only appears during two of the 50 frames in the recording. In modelling the dynamics in this region, we exclude these intermediate states and only model these four ST topologies in Fig 7. More precisely, for the six persistent nodes $\{p_i\}_1^6$ we simply assume rewiring occurs when one of the non-persistent nodes crosses the lines $\overline{p_1p_2}$ or $\overline{p_4p_5}$ and the topology changes to be the closest to that in Fig 7. We use the same parameters σ, a as in Region I to perform numerical solutions of the Langevin equation (1). Fig 6(bottom) and Fig S6 show that these simulations agree well with abstracted graphs in terms of the angle distribution for the non-persistent nodes, the time-dependent total length and dynamics of non-persistent nodes.

3.3 ER remodelling in the control

The previous section demonstrates that the treated ER network is well modeled as a perturbed ESN where the terminals correspond to the persistent nodes and perturbation is due to Brownian motion. The control ER network can also be viewed as a perturbed ESN as illustrated in Fig 5 where terminals include persistent and degree one nodes. However, the perturbation in the control is of higher amplitude and more heterogeneous than Brownian motion. The perturbations include Brownian forces, but streaming and organelle motion also have a major effect on the network structure. Indeed, the dynamics of the control ER network is much richer than that in the treated case and we have not yet attempted to model

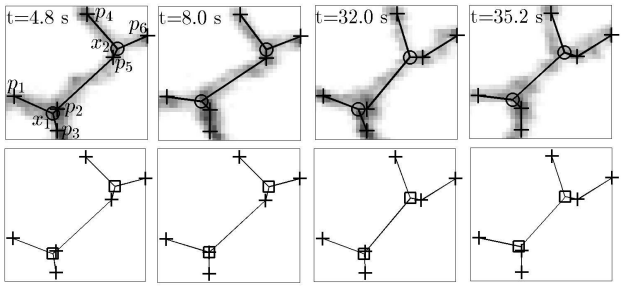

Figure 7: Top: four different graph structures from treated ER network at different time for Region II in Fig 1(b). The $p_i (i = 1, \cdots, 6)$ indicate the locations of six persistent nodes while $x_{1,2}$ indicate the locations of two non-persistent nodes. Bottom: four Steiner trees correspond to the abstracted graphs shown above. The marker '+' indicates persistent, 'o' indicates non-persistent nodes and 'square' indicates the Steiner points. The imaging data is taken from [9].

the full dynamics of the control ER network even for restricted regions, but we do illustrate some of the challenges and the complexity of the dynamics.

One problem in interpreting the dynamics of the control ER network is that some of the persistent nodes may only be visible for part of the sequence - there appear to be moments that detachment/reattachment of the ER network occurs. This may lead to incorrect classification of persistent points or terminals as non-persistent nodes. For example, Fig 8(a) show two nodes $p_{1,2}$ that only persistently appear for a proportion of the recording. This suggests that for the control ER network persistent nodes can be dynamically appearing and disappearing from the network.

In addition, in the control sample the ER network undergoes more structural changes which can be much more complex than in the treated ER network. Phenomenon such as node splitting to create new degree one nodes, opening and closing of loops, creation of new junctions and destruction of nodes as well as edges (filaments) are all observed in the control. Fig 8 illustrate some examples of these phenomenon in ER network remodelling.

3.4 Estimation of ER filament tension and cytoplasm viscosity from the model

We use the Langevin model (1) and the estimated parameters discussed in Section 3.2 to obtain estimates for the ER filament tension force and the local effective viscosity, at least for the treated ER in Region I. The inertial forces involved are negligible and we make the following assumptions: (A1) We suppose that the ER filaments are approximately cylindrical with constant radius R and surface tension γ; this means that the tension force $F := 2\pi R\gamma$ is approximately constant in the ER filaments. (A2) We suppose that the environment outside the ER filament is fluid with constant effective viscosity η. (A3) We suppose that the ER junction can be approximated as a sphere of radius R that is acted on purely by Stokes drag, filament tension and Brownian forces.

For Region I and dynamics discussed in Section 3.2.1, the non-persistent node $x(t) \in \mathbf{R}^2$ moves so that the tension and Stokes drag forces balance the Brownian forces; hence $x(t)$

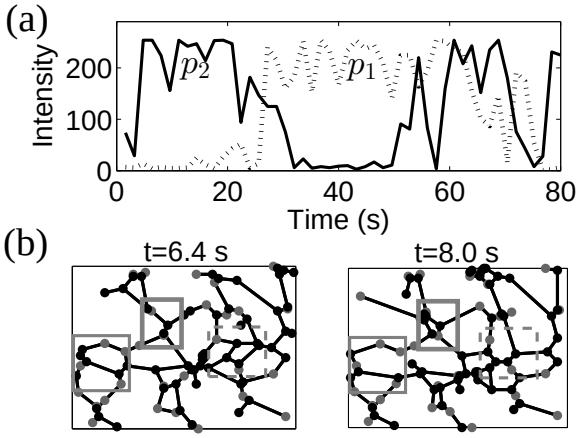

Figure 8: (a): the time-dependent maximal GFP intensity in a small neighborhood (with a radius distance of 3 pixels) indicating two persistent nodes $p_{1,2}$ only visible for part of the sequence. (b): two consecutive networks at a chosen region in the native state illustrating examples of complex remodelling. The thick rectangle shows a region where loop closing occurs (branching also takes place); the thin rectangle shows a loop opening; the dashed rectangle shows a complex structural change that will presumably be resolved only using a higher time resolution movie.

satisfies the Langevin equation

$$F\nabla_x f(x) + 6\pi\eta R\frac{dx}{dt} = \sqrt{2k_BT6\pi\eta R}\xi(t). \tag{5}$$

where k_B is the Boltzmann's constant and T is the temperature [34]. This reduces to Eq (1) with

$$a = \frac{F}{6\pi\eta R} \text{ and } \sigma = \frac{k_BT}{6\pi\eta R}. \tag{6}$$

The ER filament diameter is measured to be $D := 2R = 0.06\mu m$ [35] and the estimated diffusion coefficient $\sigma \approx 0.008 \pm 0.001\mu m^2$ is comparable to $\sim 10^{-4}\mu m^2/s$ measured for organelles of size $\sim 0.1\mu m$ [36]. Using $T = 298K$ $D := 2R = 0.06\mu m$ and the estimated parameters a, σ from Section 3.2.1, the relations (6) gives an effective viscosity η and tension force F for the situation in Region I that are

$$\eta \approx 909 \pm 113.7cP \text{ and } F \approx 0.1 \pm 0.02pN \tag{7}$$

where the error is from propagation of uncertainty [37] in drift and diffusion coefficients. However, Fig 9 suggests that the time resolution means we are in the region of elastic behaviour and the estimate of viscosity is overestimated. In particular, the mean square displacement of the ER junction in Region I is almost independent of time lag; see Fig 9(right). This suggests that the time resolution in the ER movie is in the region of elastic behaviour and at this measured time scale the cytoplasm behaves predominantly elastic. Thus the effective viscosity $\eta = 909cP$ from (7) is merely an upper bound. It is well known that the cytoplasm displays both elastic and viscous characteristics [13, 14] depending on the particle length scale in comparison to the cytoskeleton; for a smaller length scale, the interstitial liquid is

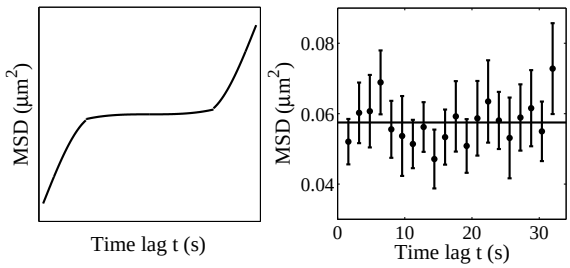

Figure 9: Left: a schematic graph for the mean square displacement (MSD) of particles in the viscoelastic cytoplasm which behaves as viscous liquid at long timescales ($t > t_2$), elastic solid at intermediate timescales ($t_1 < t < t_2$) and viscous again at short time scale ($t < t_1$). Right: MSD of the non-persistent node in Region I highlighted in Fig 1(b) shows almost no dependence on time lags in a range of $[1.6s, 32s]$ with an average of $0.0575\mu m^2$; bar shows the error of the mean. The MSD of the node movement for a time lag $t = k\delta$ is approximated as $\sum_{n=1}^{N-k} |x((n+k)\delta) - x(n\delta)|^2/(N-k)$.

only viscous, while for a larger length scale as illustrated in Fig 9(left) that the cytoplasm is predominantly viscous at long time scales ($t > t_2$) and predominantly elastic at short time scales ($t_1 < t < t_2$), and behaves again as a viscous liquid at time scales $t < t_1$.

4 DISCUSSION

Previous quantitative descriptions of ER network geometry have been restricted to fairly rudimentary measures of filament length and static elements. ER network remodelling and the dynamic nature of this process have not been adequately quantitatively described. Questions relating to whether all ER filaments are under constant tension and whether filament formation is constrained so that the entire network maintains a minimal length are unanswered. By understanding these basic principles it provides a platform from which to determine and measure the effects of the molecular components controlling such events. Here, using experimental data from plants we have shown that the ER network is constrained and is well-modelled as minimal networks that are perturbations of ESNs where the perturbations apparently involve random (Brownian) and deterministic (streaming and organelle motion) forces. The treated ER network is particularly amenable to this analysis in that the structure seems to be approximately constant over longer periods than for the control and the network topology only changes locally.

This modelling approach has been validated by quantitative comparison of the dynamical networks extracted from the biological data, including the network length, displacement of junctions, and angle distributions of the junctions in the networks. This has enabled us to estimate the tension force of the ER network (and to a certain extent, the viscosity of the cytoplasm) simply from observing the sequences of images. Higher time and space resolution imaging should improve the accuracy of these estimates.

Many questions remain unanswered and we discuss some of these below. Firstly, the mechanisms that regulate ER reorganization and remodelling are poorly understood. Better quantitative tools providing details on parameters relating to remodelling are required. Note

that the distributions of the total length in Region I and Region II differ. Even in the treated condition where ER dynamics are restricted (e.g. Fig 7) the structural changes still remain unclear, though additional branching points can transiently appear (e.g. Fig S7). It would be particularly interesting to using higher temporal and spatial resolution imaging so that one can study, for example, the transitions between different topologies. A statistical model (e.g. for the total length of the network) would help quantify the network topologies and large deviation theory could be used to quantify how often major topological changes are undergone by the network.

Secondly, several of the physical processes that determine the structure of the ER network in living cells are unclear. Our estimations of filament tension and viscosity using assumptions A1-A3 gives a low diffusion coefficient (relatively high effective viscosity) and low tension force compared for example to molecular motor stall forces or tether force estimated in [12]. A low tension force could be expected as it allows dynamical remodelling of ER junctions under perturbations. However, the physical environment is much more complex. Both the vacuole and plasma membrane undergo dynamical surface alterations (local shape changes and deformation for vesicle exchange). The quasi 2D like cytoplasmic region (which can also transverse the cell in trans vacuolar strands that 'pierce' and run through the vacuole) is packed with membrane bound organelles, vesicles, protein complexes, cytoskeletal filaments and macromolecules (such as carbohydrates). All of these substructures within the cytoplasm are not static and appear to undergo seemingly random motion; the plant cytoplasm is known to be a highly heterogeneous environment and the assumptions A1-A3 are likely to be challenged by further collection of data.

It may well be that tensions and filament diameter may vary around the network; nevertheless, assumption A1 could be experimentally explored *in vitro* and *in vivo*; assumption A2 could be measured by comparing the fluctuations of shorter ER filaments if spatial resolution is increased to the point that these fluctuations can be resolved. Assumption A3 will be modified in the presence of other forces, for example tethering forces to organelles or the cytoskeleton, and it could be improved by more detailed modelling of the membrane geometry at such junctions, though this is likely to be computationally challenging. Detailed considerations of the motion of the filaments themselves (and not just the junctions) is likely to give a better but less tractable model.

Finally, although the Langevin equation (5) seems to model the treated ER dynamics well, it will be much harder to model the control ER dynamics without considerably more data at a higher spatial and temporal resolution. The remodelling discussed in Section 3.3 includes the extension/retraction of actin tubules and motion of organelles as well as interactions with regions of cytoplasmic streaming and drastic rearrangements of the entire ER; the topology can change substantially between frames and this is not resolved for example in Movie 2; this is evident from Fig 8 where significant reorganization has taken place between two frames of the movie.

SUPPLEMENTARY MATERIAL

This supplementary material gives some details of the image processing method, network analysis, and parameter estimation for the Langevin modelling as well as some details of the

Movies 1 and 2.

ACKNOWLEDGMENTS

The authors thank "Bringing the Gaps; the Exeter Science Exchange" funded as EPSRC grant EP/I001433/1 for support that led to the inception of this project, to BBSRC grant BB/J009903/1 for partial support for CL. We also thank the following individuals for some very interesting conversations related to this work: Vadim Biktashev, Larry Griffing, Gero Steinberg and Peter Winlove.

References

[1] Levine, T., and C. Rabouille. 2005. Endoplasmic reticulum: one continuous network compartmentalized by extrinsic cues, *Curr. Opin. Cell. Biol.* 17:362-368.

[2] Lynes, E. M., and T. Simmen. 2011. Urban planning of the endoplasmic reticulum (ER): How diverse mechanisms segregate the many functions of the ER, *Biochim. Biophys. Acta* 1813:1893-1905.

[3] Roussel, B. D., A. J. Kruppa, E. Miranda, D. C. Crowther, D. A. Lomas, and S. J. Marciniak. 2013. Endoplasmic reticulum dysfunction in neurological disease. *Lancet Neurol.* 12:105-118.

[4] Viana, R. J., A. F. Nunes, and C. M. Rodrigues. 2012. Endoplasmic reticulum enrollment in Alzheimer's disease, *Mol Neurobiol.* 46:522-534.

[5] Goyal, U., and C. Blackstone. 2013. Untangling the web: Mechanisms underlying ER network formation *Biochim Biophys Acta.* 1833:2492-2498.

[6] Sparkes, I., C. Hawes, and L. Frigerio. 2011. FrontiERs: movers and shapers of the higher plant cortical endoplasmic reticulum. *Curr. Opin. Plant Biol.* 14:658-665.

[7] Sparkes, I. A., T. Ketelaar, N. C. de Ruijter, and C. Hawes. 2009. Grab a Golgi: laser trapping of Golgi bodies reveals in vivo interactions with the endoplasmic reticulum. *Traffic* 10:567-71.

[8] Friedman, J. R., and G. K. Voeltz. 2011. The ER in 3D: a multifunctional dynamic membrane network. *Trends in Cell Biology* 21:709-717.

[9] Sparkes, I. A., J. Runions, C. Hawes, and L. Griffing. 2009. Movement and Remodeling of the Endoplasmic Reticulum in Nondividing Cells of Tobacco Leaves. *Plant Cell* 21:3937-3949.

[10] Griffing, L., H. T. Gao, and I. Sparkes. 2014. ER network dynamics are differentially controlled by myosins XI-K, XI-C, XI-E, XI-I, XI-1 and XI-2. *Front. Plant Sci.* 5:218.

[11] Ueda, H., E. Yokota, N. Kutsuna, T. Shimada, K. Tamura, T. Shimmen, S. Hasezawa, V. V. Dolja, and I. Hara-Nishimura. 2010. Myosin-dependent endoplasmic reticulum motility and F-actin organization in plant cells. *Proc. Natl. Acad. Sci. U.S.A.* 107:6894-6899.

[12] Upadhyaya, A., and Sheetz, M. P. 2004. Tension in tubulovesicular networks of Golgi and endoplasmic reticulum membranes. *Biophys. J.* 86:2923-2928.

[13] Tseng, Y., Kole, T.P., and Wirtz, D. 2002. Micromechanical mapping of live cells by multiple-particle-tracking microrheology. *Biophys J* 83:3162-3176.

[14] Wirtz, D. 2009. Particle-tracking microrheology of living cells: principles and applications. *Annu. Rev. Biophys.* 38:301-326.

[15] Radochová, B., J. Janáček, K. Schwarzerová, E. Demjénová, and Z. Torori. 2005. Analysis of endoplasmic reticulum of tobacco cells using confocal microscopy. *Image Anal. Stereol.* 24:181-185.

[16] Puhka, M., H. Vihinen, M. Joensuu, and E. Jokitalo. 2007. Endoplasmic reticulum remains continuous and undergoes sheet-to-tubule transformation during cell division in mammalian cells. *J. Cell Biol.* 179:895-909.

[17] Puhka, M., M. Joensuu, H. Vihinen, I. Belevich, and E. Jokitalo. 2012. Progressive sheet-to-tubule transformation is a general mechanism for endoplasmic reticulum partitioning in dividing mammalian cells. *Mol. Biol. Cell* 23: 2424-2432.

[18] West, M., N. Zurek, A. Hoenger, and Gia K. Voeltz. 2011. A 3D analysis of yeast ER structure reveals how ER domains are organized by membrane curvature. *J. Cell Biol.* 193:333-346.

[19] Griffing, L. R. 2010. Networking in the endoplasmic reticulum. *Biochem. Soc. Trans.* 38:747-753.

[20] Sparkes, I., L. Frigerio, N. Tolley, and C. Hawes. 2009. The plant endoplasmic reticulum: a cell-wid web. *Biochem. J.* 423:145-155.

[21] Bouchekhima, A. N. 2009. *Quantification of the Plant Endoplasmic Reticulum*, PhD thesis, University of Warwick.

[22] Bouchekhima, A. N., L. Frigerio, and M. Kirkilionis. 2009. Geometric quantification of the plant endoplasmic reticulum. *J. of Microscopy* 234:158-172.

[23] Park, S. H., and G. Blackstone. 2010. Further assembly required: construction and dynamics of the endoplasmic reticulum network. *EMBO Rep.* 11:515-521.

[24] Fomenko, A. T. 1989. The Plateau Problem: Historical Survey. Williston, VT: Gordon & Breach.

[25] Terasaki, M., T. Shemesh, N. Kasthuri, R. K. Klemm, R. Schalek, K. J. Hayworth, A. R. Hand, Maya. Yankova, G. Huber, J. W. Lichtman, T. A. Rapoport, K. M. Kozlov. 2013. Stacked endoplasmic reticulum sheets are connected by helicoidal membrane motifs. *Cell* 154:285-296.

[26] Courant, R., and H. Robbins. 1941. What Is Mathematics?, Oxford University Press, New York.

[27] Hwang, F. K., D. S. Richards, and P. Winter. The Steiner tree problem. *Annals of Discrete Mathematics*. Vol. 53. Elsevier Science Publishers B.V., North-Holland, Amsterdam (1992)

[28] GeoSteiner is a software for computing Steiner trees and is available from `http://www.diku.dk/hjemmesider/ansatte/martinz/geosteiner/`.

[29] Guo, Z., and R. W. Hall. 1989. Parallel thinning with two-subiteration algorithms. *Comm. ACM.* 32:359-373.

[30] Øsendal, B. 1998. Stochastic Differential Equations. An Introduction with Applications, 5th ed., Springer-Verlag, Berlin.

[31] Barndorff-Nielsen, OLE E., and N. Shephard. 2003. Realized power variation and stochastic volatility models. *Bernoulli*. 9:243-265.

[32] Yoshida, N. 1992. Estimation for Diffusion Processes from Discrete Observation. *J. Multivar. Anal.* 41:220-242.

[33] Newey W. K., and D. McFadden. 1994. Chapter 35: Large sample estimation and hypothesis testing. In Handbook of Econometrics, Vol.4. Robert Engle and Daniel McFadden editors, Elsevier, North Holland.

[34] Coffey, W. T., and Y. P. Kalmykov. The Langevin Equation: With Applications to Stochastic Problems in Physics, Chemistry and Electrical Engineering (Third edition), World Scientific Series in Contemporary Chemical Physics - Vol 14.

[35] Shibata, Y., J. Hu, M. M. Kozlov, and T. A. Rapoport. 2009. Mechanisms Shaping the membranes of Cellular Organelles. *Annu. Rev. Cell Dev. Biol.* 25:329-354.

[36] Manneville, J., S. Etienne-Manneville, P. Skehel, T. Carter, D. Ogden, and M. Ferenczi. 2003. Interaction of the actin cytoskeleton with microtubules regulates secretory organelle movement near the plasma membrane in human endothelial cells. *Journal of Cell Science*. 116:3927-3938.

[37] Taylor, J. R. 1997. An Introduction to Error Analysis: The Study of Uncertainties in Physical Measurements, University Science Books; 2rd edition.